

Coherent detection of hidden spin-lattice coupling in a van der Waals antiferromagnet

Emre Ergeçen^{1,*}, Batyr Ilyas^{1,*}, Junghyun Kim^{2,3}, Jaena Park^{2,3}, Mehmet Burak Yilmaz¹, Tianchuang Luo¹, Di Xiao^{4,5}, Satoshi Okamoto⁶, Je-Geun Park^{2,3}, and Nuh Gedik^{1,†}

¹Department of Physics, Massachusetts Institute of Technology, Cambridge, 02139, Massachusetts, USA; ²Center for Quantum Materials, Seoul National University, Seoul 08826, Republic of Korea.; ³Department of Physics and Astronomy and Institute of Applied Physics, Seoul National University, Seoul 08826, Republic of Korea.; ⁴Department of Materials Science and Engineering, University of Washington, Seattle, Washington, USA; ⁵Department of Physics, University of Washington, Seattle, Washington, USA; ⁶Materials Science and Technology Division, Oak Ridge National Laboratory, Oak Ridge, Tennessee 37831 USA

Strong interactions between different degrees of freedom lead to exotic phases of matter with complex order parameters and emergent collective excitations. Conventional techniques, such as scattering and transport, probe the amplitudes of these excitations, but they are typically insensitive to phase. Therefore, novel methods with phase sensitivity are required to understand ground states with phase modulations and interactions that couple to the phase of collective modes. Here, by performing phase-resolved coherent phonon spectroscopy (CPS), we reveal a hidden spin-lattice coupling in a vdW antiferromagnet FePS₃ that eluded other phase-insensitive conventional probes, such as Raman and X-ray scattering. With comparative analysis and analytical calculations, we directly show that the magnetic order in FePS₃ selectively couples to the trigonal distortions through partially filled t_{2g} orbitals. This magnetoelastic coupling is linear in magnetic order and lattice parameters, rendering these distortions inaccessible to inelastic scattering techniques. Our results not only capture the elusive spin-lattice coupling in FePS₃, but also establish phase-resolved CPS as a tool to investigate hidden interactions.

Ultrafast spectroscopy | van der Waals magnets | Spin-phonon coupling

Van der Waals (vdW) materials and their heterostructures host tunable correlated phenomena, which arise from the interplay between lattice, spins and orbitals, ranging from unconventional superconductivity (1) to charge-ordered states (2). In particular, vdW magnets have recently emerged as platforms to study strong interactions between lattice and spins (3–5). For example, the stacking configuration of two adjacent layers can tune the interlayer exchange interaction (6), leading to diverse magnetic ground states (7), such as the coexistence of two distinct magnetic states with a mesoscopic periodicity defined by the twist angle (8–10).

Despite a plethora of phases that emerge from strong spin-lattice coupling in vdW magnets, their microscopic origins are not well understood and demand new techniques with magnetic and structural sensitivity. This is especially true for FePS₃ (Figure 1a), a prototypical vdW antiferromagnet, which exhibits easy-axis zigzag antiferromagnetic order below its Néel temperature ($T_N=118$ K) (11). FePS₃ displays an unusual set of magnetically active low energy collective modes (12–15), interpreted as zone folded phonon modes, indicating strong spin-lattice coupling. However, the structural phonon modes that exist above the Néel temperature do not experience any frequency renormalization, a hallmark of strong spin-phonon coupling (16, 17), despite the emergence of new magnetically enabled phonons at the onset of magnetic order. The microscopic mechanisms leading to the dichotomy between new collective modes and structural phonon modes,

and the nature of spin-lattice coupling in FePS₃ still remain an open question.

In this work, we employ phase-resolved coherent phonon spectroscopy (CPS) to reveal a mode selective spin-lattice coupling in FePS₃ that remained hidden to Raman and X-ray scattering experiments (12, 14, 15). CPS resolves both the amplitudes and the phases of the phonons in FePS₃ by coherently driving them and visualizing their oscillations in real time. Below the Néel temperature (T_N) of FePS₃, this elusive spin-lattice interaction manifests itself as a sudden change in the phase and amplitude of the 7.51 THz phonon mode. We found that this interaction is mode-specific, as the 11.45 THz phonon mode does not show any change in its phase or amplitude. In order to pin down the origin of this mode-selective change, we compare and contrast our experimental results with NiPS₃, which is isostructural to FePS₃ (18, 19). Using crystal field calculations, we find the origin of this effect as a magnetoelastic coupling between t_{2g} orbitals and trigonal distortion, which overlaps strongly with the symmetry of the 7.51 THz A_{1g} mode. Finally, our analysis identifies the origin of the observed mode-specific spin-phonon coupling in FePS₃, and hence resolves the dichotomy between low energy and structural collective modes.

In our experimental scheme (Figure 1a), a low intensity and ultrashort pump pulse displacively excites the coherent

Significance Statement

With the advent of van der Waals (vdW) materials, emergent phases of matter started to themselves themselves in two-dimensional devices. In particular, vdW magnets show strong interactions between lattice and spins, leading to diverse magnetic ground states. Our work provides a definitive mechanism to spin-lattice coupling in vdW magnets, FePS₃ and NiPS₃, by employing phase resolved coherent phonon spectroscopy. We observe sudden change in the phase of a specific phonon, undetectable by phase-insensitive conventional techniques, such as Raman and X-ray scattering. Our work directly establishes the role of trigonal distortions and d-orbital occupation in spin-lattice coupling in vdW magnets.

E.E., B.I. and M.B.Y. built the optical spectroscopy setups. E.E. and B.I. performed the experiments. E.E., B.I. and N.G. analysed and interpret the data with crucial inputs from T.L. E.E. developed the theoretical model under the supervision of D.X. and S.O. J.K. and J.P. synthesized and characterized single crystals of FePS₃, supervised by J.-G.P. E.E., B.I. and N.G. wrote the manuscript with crucial inputs from all authors. This project was supervised by N.G.

The authors declare no competing interests.

* E.E. (Author One) contributed equally to this work with B.I. (Author Two).

† To whom correspondence should be addressed. E-mail: gedik@mit.edu

phonons of FePS₃ with A_{1g} and E_g symmetries without destroying the magnetic order (Methods). After the pump excitation, a lower intensity probe pulse tracks the coherent phonon oscillations as a function of pump-probe delay time Δt . The center wavelength of the pump is 760 nm (1.63 eV) and the pulse bandwidth is 60 nm. In this energy range, our broadband photoexcitation overlaps with the charge transfer gap (20, 21). Figure 1c shows the transient reflectivity trace of FePS₃ at room temperature. In addition to the incoherent electronic decay, the signal consists of an oscillatory part composed of two Fourier components (Figure 1c inset), with frequencies of 7.51 THz and 11.45 THz. The lattice distortions corresponding to these phonon modes of A_{1g} symmetry are shown in Figure 1b. The 7.51 THz mode is an out-of-plane breathing mode of sulfur atoms, whereas the 11.45 THz mode involves the in-plane motion of sulfur atoms.

To investigate the effects of spin-lattice coupling on the coherent phonon spectrum, we performed temperature dependent phase-resolved CPS on FePS₃ and traced the changes in transient reflectivity as a function of temperature (Figure 2a). Around 90 K, the signal develops a long-lived component, indicating a change in electronic structure due to the magnetic order. Concurrent with this change, we observe a change in coherent phonon oscillations (Figure 2a), which are extracted by subtracting the incoherent background with a single exponential fit. Figure 2b shows the temperature-dependent Fourier transform of the coherent phonon oscillations. Below ~ 90 K, coherent phonon spectrum develops a new mode at 3.28 THz. This low energy mode has been observed in Raman spectroscopy below T_N and attributed to magnetic zone-folding (12, 15), heralding the onset of magnetic order. We use this mode as a proxy for magnetic order in our experimental scheme. We attribute the discrepancy between the reported Néel temperature (118K) and the observed Néel temperature (90 K) to steady-state laser induced average heating in our experiment, due to high repetition rate of our laser. As shown in Figure 2b and 2c, simultaneously with the emergence of the 3.28 THz mode and hence with the onset of the magnetic order, the 7.51 THz mode amplitude shows a clear downturn. Upon cooling, this coherent phonon oscillation vanishes at around 80 K and recovers with further cooling. The 11.45 THz mode, on the other hand, shows negligible change across T_N.

We further examine the time-domain evolution of these modes by performing Fourier filtering. The filtered spectral region and the respective time traces are given in Figure 2b. Strikingly, the 7.51 THz mode exhibits a π phase shift at low temperatures, which is absent in the 11.45 THz phonon mode, as shown in Figure 2c. Figure 2c also shows the phase-corrected coherent phonon amplitudes, where the π phase shift corresponds to negative mode amplitude. The 3.28 THz phonon mode shows an order parameter behaviour, indicating that the pump pulse does not destroy the magnetic order at all temperatures. The 7.51 THz mode amplitude starts to decline at the onset of magnetic order, and its decrease follows the same order parameter behaviour as the 3.28 THz one. This behaviour is strongly suppressed in the 11.45 THz phonon mode, suggesting a smaller magnetoelastic coupling compared to the 7.51 THz mode.

The frequencies of both phonon modes are in agreement with the Raman results. However, in contrast to CPS, the

Raman scattering amplitudes for the 7.51 THz and 11.45 THz modes do not show any temperature dependence (SI Figure 2). Despite the sensitivity of both Raman and CPS to phonon modes, both methods excite and detect phonons differently. Raman scattering measures phonon induced changes in polarizability, also known as Raman matrix element ($|\frac{\partial \epsilon}{\partial Q}|^2$) by making a transition between the ground state and the single phonon excited state (22). This implies that in FePS₃, the Raman matrix elements of both A_{1g} phonons remain constant at all temperatures. Contrary to Raman spectroscopy, CPS relies on pump induced coherent phonons generated through displacive or impulsive processes (23). Thus, the observed mode amplitude in CPS is equal to:

$$R_{osc} = \sum_i \frac{\partial R}{\partial \epsilon} \frac{\partial \epsilon}{\partial Q_i} \Delta Q_i \quad [1]$$

where ΔQ_i corresponds to the initial displacement of a phonon after photoexcitation, ϵ is the dielectric constant and R is the reflectivity as a function of dielectric constants. As the Raman matrix elements stay the same at all temperatures, the temperature dependent amplitude and phase changes in CPS can be attributed to the change in ΔQ_i .

To gain more insights into the physical origins leading to the mode-selective and magnetic order-dependent phonon phase shift in FePS₃, we study the free energy landscape before and after the photoexcitation. For ultrafast excitation, the initial phonon displacement ΔQ equals the difference between the minimal energy lattice positions before and after pump excitation. This mechanism, also known as displacive excitation of coherent phonons, for FePS₃ is shown in Figure 3, where the upper and lower free energy manifolds represent photoexcited and equilibrium states, respectively. Above T_N, the equilibrium and photoexcited free energy landscapes have different minima because of the presence of excited electrons. Below T_N, the equilibrium atomic positions shift due to magnetoelastic coupling, and the amount of displacement along specific mode direction depends on the strength of the mode selective spin-phonon coupling. In this case, the pump excitation perturbs the magnetic order and causes the magnetoelastic coupling to relax, leading to an excited free energy manifold similar to the one above T_N. If the magnetoelastic coupling is linear in phonon position operators, the magnetic order alters the coherent phonon displacements and phases without changing their frequencies and Raman matrix elements, as shown in Figure 3. The mathematical form of the phenomenological free energy describing this scenario is given in SI. Because the 7.51 THz phonon mode shows a much larger change than the 11.45 THz phonon mode concurrent with the magnetic order, we can explain our experimental findings with the fact that the magnetoelastic coefficient of the 7.51 THz mode is significantly higher than that of the 11.45 THz mode.

Even though our phenomenological model captures our experimental observations with a mode-selective spin-lattice coupling model, it does not provide a microscopic reason for its mode-specificity and the linear coupling between the phonons and magnetic order. To pin down the microscopic origin of these observations, we compare the coherent phonon spectra of FePS₃ to that of NiPS₃, which is isostructural to FePS₃. Both systems develop a zigzag AFM order with similar exchange coupling constants (24–26). In addition to their magnetic structures, the optical spectra reflect similar bandgap for

both (20, 27, 28). The significant difference between these two systems are in the electronic configuration of transition metal ions. Ni²⁺ ions (3d⁸) have two more d-electrons than the Fe²⁺ ions (3d⁶). Although the CPS spectra of NiPS₃ (see Figure S3) exhibit both 7.51 and 11.45 THz phonon modes with the same symmetry as FePS₃, none of these modes show any temperature-dependent phase or amplitude change below T_N. Therefore, we can ascribe the mode-selective spin-lattice coupling in FePS₃ to its localized d-orbital electron configuration.

The d-orbital electron configurations of Ni²⁺ and Fe²⁺ ions are given Figure 4a. In both compounds, transition metal ions are surrounded by ligands with octahedral arrangements, together with trigonal distortions (19). Both Fe²⁺ and Ni²⁺ ions have two unpaired spins in e_g orbitals. However, t_{2g} levels in Fe²⁺ are partially-filled, and in Ni²⁺, these levels are fully-filled. Therefore we can narrow down the microscopic origin of the mode-selective magnetoelasticity in FePS₃ to t_{2g} orbitals.

To examine the magnetoelastic effects in FePS₃, we theoretically analyze the system on a single octahedra level and focus on the low energy t_{2g} manifold. In the presence of trigonal distortions, the Hamiltonian for the low energy t_{2g} manifold can be written as (19):

$$H = (\Delta_{\text{trig.}} + \alpha u)L_z^2 + \lambda LS + \frac{1}{2}Bu^2 \quad [2]$$

where $\Delta_{\text{trig.}}$ is the existing trigonal splitting, λ is the spin-orbit coupling constant, B is the elastic constant associated with trigonal distortions, and α quantifies the change in energy following a change in trigonal distortions. The quantization axis is along the (111) direction of the octahedra and the c-axis of the crystal. Despite the absence of a direct coupling between the structural distortion u and the spin operator S , spin-orbit coupling gives rise to an effective Hamiltonian, that is proportional to $H_{\text{eff, magnetoelastic}} = -\frac{\alpha\lambda^2}{\Delta^2}uS_z^2$. This term implies that the z-component of spins selectively displaces the octahedra along the trigonal distortion. This does not cause any change in its elastic properties, which would appear as a coupling quadratic term in u and would alter the normal mode frequencies. Furthermore, this microscopic treatment yields the value of trigonal distortion as $u_0 = \frac{\alpha\lambda^2}{B\Delta^2}S_z^2$. Following the pump excitation, this value will get altered because of the pump induced perturbation of the magnetic system, which is equal to $\delta u_0 = \frac{2\alpha\lambda^2}{B\Delta^2}S_z\delta S_z$. This expression is identical to the magnetic order-dependent phonon displacement (ΔQ) expression and explains the spin-dependent coherent phonon oscillations microscopically on a single ion level.

Our microscopic analysis of mode-selective magnetoelasticity that relies on single ion anisotropy is valid for FePS₃ on the bulk level. First, below the magnetic transition, the expectation value of S_z^2 is constant for different octahedra composing the material. Therefore, each individual layer of FePS₃ undergoes a uniform trigonal distortion, and S_z operator can be replaced with the antiferromagnetic order parameter N . Furthermore, the spin-orbit coupling in this material emerges from on-site e_g d-orbitals. Unlike other vdW magnets such as CrI₃ (29, 30), the spin-orbit coupling does not emerge from ligands, rendering our single-ion treatment valid for FePS₃ on the bulk level.

The trigonal distortions induced by the mode-selective magnetoelasticity on the single octahedra level correspond to out-

of-plane motion of sulfur atoms on the bulk level. Therefore, the mode-selective magnetoelasticity will couple to phonon modes differently, depending on their spatial projection on the trigonal distortion or out-of-plane motion of sulfur atoms. As shown in Figure 1, 7.51 THz A_{1g} phonon mode modulates the out of plane distance of sulfur atoms and directly corresponds to the trigonal distortion of octahedra. On the other hand, as the 11.45 THz phonon mode involves in-plane motion of sulfur atoms, the coupling between this phonon mode and the trigonal distortions is negligible. Furthermore, as shown in Figure 4b, this magnetoelastic coupling and phonon phase shift are absent in NiPS₃ because of the fully filled t_{2g} orbitals.

In summary, using coherent phonon spectroscopy, we reveal mode selective magnetoelasticity in FePS₃, which previously eluded phase insensitive measurements. This effect changes the coherent phonon amplitude and the phase of the 7.51 THz A_{1g} phonon mode without frequency renormalization below the magnetic transition temperature. By performing a comparative study between FePS₃ and NiPS₃, we pinpoint the mode selective origin of spin-lattice coupling and show the pivotal role of trigonal distortions in these compounds. Our results not only reveal a mode selective magnetoelasticity in FePS₃ but resolve the dichotomy between magnetically enabled phonon modes and already existing phonon modes. Our results suggest that perturbations that directly couple to the trigonal distortions in FePS₃, such as pressure (31) and nonlinear phononics (32, 33), can be used to manipulate the magnetic order or to enter nonequilibrium magnetic phases which cannot be accessed in equilibrium. Furthermore, we envision that the coherent phonon spectroscopy technique can be utilized as a highly sensitive probe of hidden spin-lattice coupling in vdW magnet monolayers and other systems with strong spin-lattice coupling.

Materials and Methods

Sample preparation. We synthesized our FePS₃ crystals using a chemical vapor transport method (for details see Ref. (34)). All the powdered elements (purchased from Sigma-Aldrich): iron (99.99% purity), phosphorus (99.99%) and sulfur (99.998%), were prepared inside an argon-filled glove box. After weighing the starting materials in the correct stoichiometric ratio, we added an additional 5 wt of sulfur to compensate for its high vapor pressure. After the synthesis, we carried out the chemical analysis of the single-crystal samples using a COXI EM-30 scanning electron microscope equipped with a Bruker QUANTAX 70 energy dispersive X-ray system to confirm the correct stoichiometry. We also checked the XRD using a commercial diffractometer (Rigaku Miniflex II). Prior to optical measurements, we determined the crystal axes of the samples using an x-ray diffractometer. We cleaved samples before placing them into high vacuum ($\sim 10^{-7}$ torr) to expose a fresh surface without contamination and oxidation.

Phase-resolved coherent phonon spectroscopy. A Ti:sapphire oscillator (Cascade-5, KMLabs), centered at 760 nm (1.63 eV) and with pulse duration of ~ 25 fs was used in our experiments. The repetition rate of the laser was set to 80 MHz. Before splitting the output into pump and probe branches, we compensated for group velocity dispersion (GVD) using a pair of chirp mirrors and N-BK7 wedges to maintain the pulse duration at the sample position. The pump and probe pulses were characterized separately at the sample position, using frequency resolved optical gating technique. The pulse duration was ~ 25 fs. To increase the signal to noise ratio of our setup, we modulate the pump intensity at 100 kHz. The probe signal from the photodiode is sent to a lock-in amplifier (Stanford Research SR830) locked to the chopping frequency (100 kHz). For faster data acquisition and averaging, the pump-probe delay is

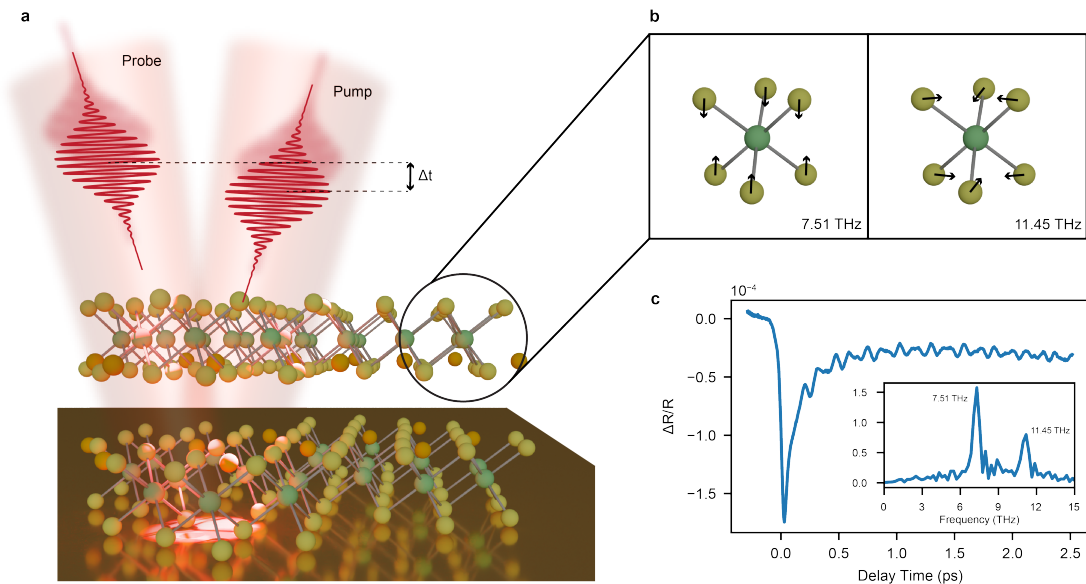


Fig. 1. Coherent phonon spectroscopy on FePS₃. **a.** An ultrashort pump pulse of 1.63 eV photon energy excites the crystal, and a subsequent probe pulse measures the transient differential reflectivity after a delay time of Δt . **b.** In FePS₃, six sulfur (yellow) atoms in an octahedral configuration surround iron (green) atoms. Arrows depict the octahedral distortions that correspond to two A_{1g} phonons with frequencies 7.51 THz and 11.45 THz. **c.** The transient reflectivity trace of FePS₃ obtained at room temperature (293 K) consists of an incoherent electronic decay signal and oscillatory features originating from coherent phonons. The Fourier spectrum (inset) of these oscillatory features reveals two phonon modes with frequencies matching the A_{1g} phonons shown in **b.**

rapidly scanned at a rate of 5 Hz with an oscillating mirror (APE ScanDelay USB). The diameters of pump and probe beam spots were 90 μm , measured by a knife edge method. The pump and probe beams are cross polarized. During all of our measurements, the pump fluence was set to 10 $\mu\text{J}/\text{cm}^2$. The detailed schematics of the setup is given in SI (Figure S1).

Data, Materials, and Software Availability. All study data are included in the article and/or supporting information.

ACKNOWLEDGMENTS. We thank Riccardo Comin for fruitful discussions. We acknowledge support from the US Department of Energy, BES DMSE (data taking and analysis) and Gordon and Betty Moore Foundation's EPIQS Initiative grant GBMF9459 (instrumentation and manuscript writing). Work at the Center for Quantum Materials was supported by the Leading Researcher Program of the National Research Foundation of Korea (Grant No. 2020R1A3B2079375). The research of S.O. was supported by the U.S. Department of Energy, Office of Science, Basic Energy Sciences, Materials Sciences and Engineering Division.

1. Y Cao, et al., Unconventional superconductivity in magic-angle graphene superlattices. *Nature* **556**, 43–50 (2018).
2. Y Xu, et al., Correlated insulating states at fractional fillings of moiré superlattices. *Nature* **587**, 214–218 (2020).
3. M Gibertini, M Koperski, AF Morpurgo, KS Novoselov, Magnetic 2D materials and heterostructures. *Nat. Nanotechnol.* **14**, 408–419 (2019).
4. B Huang, et al., Emergent phenomena and proximity effects in two-dimensional magnets and heterostructures. *Nat. Mater.* **19**, 1276–1289 (2020).
5. KS Burch, D Mandrus, JG Park, Magnetism in two-dimensional van der Waals materials. *Nature* **563**, 47–52 (2018).
6. N Sivasdas, S Okamoto, X Xu, CJ Fennie, D Xiao, Stacking-dependent magnetism in bilayer CrI₃. *Nano letters* **18**, 7658–7664 (2018).
7. B Huang, et al., Layer-dependent ferromagnetism in a van der Waals crystal down to the monolayer limit. *Nature* **546**, 270–273 (2017).
8. T Song, et al., Direct visualization of magnetic domains and moiré magnetism in twisted 2D magnets. *Science* **374**, 1140–1144 (2021).
9. Y Xu, et al., Coexisting ferromagnetic–antiferromagnetic state in twisted bilayer CrI₃. *Nat. Nanotechnol.* (2021).
10. H Xie, et al., Twist engineering of the two-dimensional magnetism in double bilayer chromium triiodide homostructures. *Nat. Phys.* (2021).

11. G Le Flem, R Brec, G Ouvrad, A Louisy, P Segransan, Magnetic interactions in the layer compounds MPX₃ (M = Mn, Fe, Ni; X = S, Se). *J. Phys. Chem. Solids* **43**, 455–461 (1982).
12. JU Lee, et al., Ising-Type Magnetic Ordering in Atomically Thin FePS₃. *Nano Lett.* **16**, 7433–7438 (2016).
13. D Lançon, et al., Magnetic structure and magnon dynamics of the quasi-two-dimensional antiferromagnet FePS₃. *Phys. Rev. B* **94** (2016).
14. M Scagliotti, M Jouanne, M Balkanski, G Ouvrad, G Benedek, Raman scattering in antiferromagnetic FePS₃ and FePSe₃ crystals. *Phys. Rev. B* **35**, 7097–7104 (1987).
15. A Ghosh, et al., Spin-phonon coupling and magnon scattering in few-layer antiferromagnetic FePS₃. *Phys. Rev. B* **103** (2021).
16. J Hong, A Stroppo, J Añiguez, S Picozzi, D Vanderbilt, Spin-phonon coupling effects in transition-metal perovskites: A DFT+U and hybrid-functional study. *Phys. Rev. B - Condens. Matter Mater. Phys.* **85** (2012).
17. J Vermette, S Jandl, MM Gospodinov, Raman study of spin-phonon coupling in ErMnO₃. *J. Phys. Condens. Matter* **20** (2008).
18. G Ouvrad, R Brec, J Rouxel, Structural determination of some MPS₃ layered phases (M = Mn, Fe, Co, Ni and Cd). *Mater. Res. Bull.* **20**, 1181–1189 (1985).
19. PA Joy, S Vasudevan, Magnetism in the layered transition-metal thiophosphates MPS₃ (M=Mn, Fe, and Ni). *Phys. Rev. B* **46**, 5425–5433 (1992).
20. M Piacentini, FS Khumalo, G Leveque, CG Olson, DW Lynch, X-ray photoemission and optical spectra of NiPS₃, FePS₃ and ZnPS₃. *Chem. Phys.* **72**, 61–71 (1982).
21. Q Zhang, et al., Observation of Giant Optical Linear Dichroism in a Zigzag Antiferromagnet FePS₃. *Nano Lett.* **21**, 6938–6945 (2021).
22. R Loudon, The Raman effect in crystals. *Adv. Phys.* **13**, 423–482 (1964).
23. HJ Zeiger, et al., Theory for displacive excitation of coherent phonons. *Phys. Rev. B* **45**, 768–778 (1992).
24. D Lançon, RA Ewings, T Guidi, F Formisano, AR Wildes, Magnetic exchange parameters and anisotropy of the quasi-two-dimensional antiferromagnet NiPS₃. *Phys. Rev. B* **98** (2018).
25. N Sivasdas, MW Daniels, RH Swendsen, S Okamoto, D Xiao, Magnetic ground state of semiconducting transition-metal trichalcogenide monolayers. *Phys. Rev. B - Condens. Matter Mater. Phys.* **91** (2015).
26. TY Kim, CH Park, Magnetic Anisotropy and Magnetic Ordering of Transition-Metal Phosphorus Trisulfides. *Nano Lett.* **21**, 10114–10121 (2021).
27. E Ergeçen, et al., Magnetically brightened dark electron-phonon bound states in a van der Waals antiferromagnet. *Nat. Commun.* **13**, 98 (2022).
28. S Kang, et al., Coherent many-body exciton in van der Waals antiferromagnet NiPS₃. *Nature* **583**, 785–789 (2020).
29. DH Kim, et al., Giant Magnetic Anisotropy Induced by Ligand LS Coupling in Layered Cr Compounds. *Phys. Rev. Lett.* **122** (2019).
30. JL Lado, J Fernández-Rossier, On the origin of magnetic anisotropy in two dimensional CrI₃. *2D Mater.* **4** (2017).
31. MJ Coak, et al., Emergent Magnetic Phases in Pressure-Tuned van der Waals Antiferromagnet FePS₃. *Phys. Rev. X* **11** (2021).

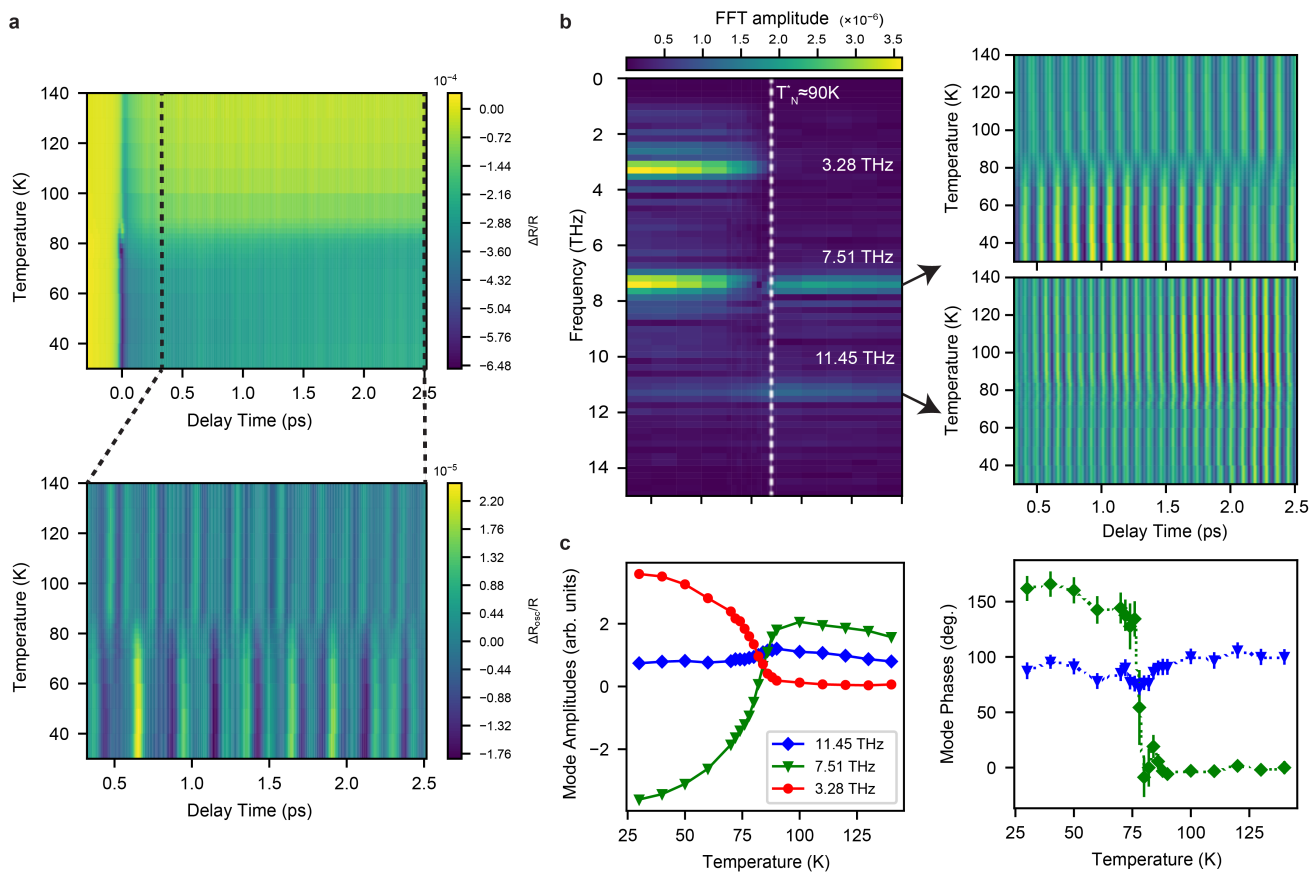


Fig. 2. The Néel order selectively couples to the 7.51 THz A_{1g} phonon mode. **a.** The temperature dependent coherent phonon spectroscopy on FePS_3 exhibits a pronounced change near ~ 90 K (upper panel). Lower panel shows the oscillatory part of the traces, extracted by fitting the incoherent background with a single exponential. **b.** (Left panel) Below ~ 90 K, in temperature dependent Fourier spectra of oscillations, a new phonon emerges mode at 3.28 THz. Fourier filtered time traces of the 7.51 THz and 11.45 THz modes are shown on the right. **c.** Temperature dependent phase-corrected amplitudes and phases of phonons. The 3.28 THz mode displays an order parameter-like behavior, and its onset is concomitant with the magnetic order. Following the emergence of this mode, the 7.51 THz mode undergoes a π -phase shift and hence its phase-corrected amplitude changes sign. The 11.45 THz mode amplitude shows no discernable change.

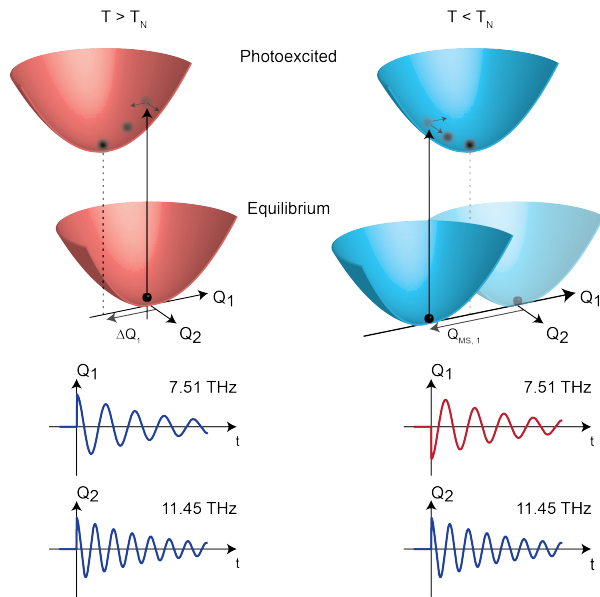


Fig. 3. Magnetoelasticity displaces the equilibrium energy landscape anisotropically and induces a mode-selective π -phase shift in coherent phonon oscillations. Upper panels show the equilibrium and photoexcited free energy landscapes. Q_1 and Q_2 are generalized atomic coordinates along the motion axis of 7.51 THz and 11.45 THz phonons, respectively. Above T_N , photoexcitation launches coherent phonons displacively due to a relative shift between photoexcited and equilibrium free energy landscape minima (e.g. ΔQ_1 along the Q_1 axis). Below T_N , magnetoelasticity induces an anisotropic shift of the equilibrium landscape, which is much stronger along the Q_1 axis ($Q_{MS,1}$) than Q_2 axis. This results in π -phase shift of the 7.51 THz mode, while 11.45 THz mode remains unaffected. This scenario is depicted in the lower panels which show the coherent oscillations of each mode in time domain below and above T_N .

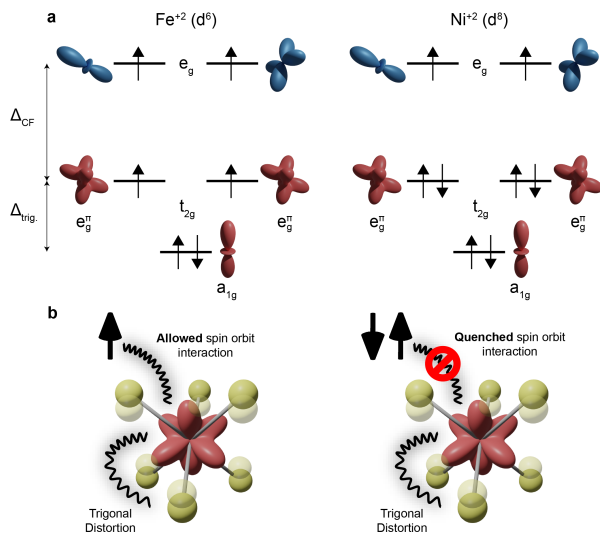


Fig. 4. Spins in e_g^π levels selectively couple to trigonal distortions and give rise to mode-selective magnetoelasticity in FePS_3 . **a.** Electronic configurations of Fe^{2+} and Ni^{2+} ions in a trigonally contracted octahedral environment of sulfur atoms. In FePS_3 , transition metal ions host two unpaired spins in e_g^π orbitals and two unpaired spins in e_g orbitals with quenched orbital angular momenta. On the other hand, in NiPS_3 , transition metal ions host two additional electrons in e_g^π orbitals compared to FePS_3 . **b.** Two unpaired spins in e_g^π orbitals of FePS_3 allow efficient coupling between the magnetic order and trigonal distortions. This magnetoelastic effect is due to spin-orbit coupling mediated virtual transitions between e_g^π and a_{1g} orbitals. This effect is absent in NiPS_3 (shown on the right), since the t_{2g} levels are fully filled.

32. AS Disa, et al., Polarizing an antiferromagnet by optical engineering of the crystal field. *Nat. Phys.* **16**, 937–941 (2020).
33. M Rodríguez-Vega, et al., Light-driven topological and magnetic phase transitions in thin layer antiferromagnets. *The J. Phys. Chem. Lett.* **13**, 4152–4158 (2022) PMID: 35507411.
34. CT Kuo, et al., Exfoliation and Raman Spectroscopic Fingerprint of Few-Layer NiPS₃ Van der Waals Crystals. *Sci. Reports* **6** (2016).